Power Electronic Devices and Components 5 (2023) 100038

Contents lists available at ScienceDirect

Power Electronic Devices and Components

journal homepage: www.journals.elsevier.com/power-electronic-devices-and-components

Hybrid model to evaluate the frequency-dependent leakage inductance of partially-filled transformers

Angshuman Sharma, Jonathan W. Kimball *

Department of Electrical and Computer Engineering, Missouri University of Science and Technology, Rolla, MO 65401, USA

ARTICLE INFO

Keywords:
Double-2-D model
Dowell's model
Hybrid model
Image method
Leakage inductance
Partially-filled transformer

ABSTRACT

The leakage inductance of a transformer designed for a power electronic converter can drop significantly as the switching frequency is increased due to skin and proximity effects. Although the magnetic image method-based double-2-D model can predict the low-frequency leakage inductance of a partially-filled transformer with sufficient accuracy, it is inherently a frequency-independent model. While Dowell's 1-D model uses frequency-dependent relations to account for both skin and proximity effects, its accuracy is severely affected by the assumed winding geometry. In this paper, a semi-analytical hybrid model is proposed that uses superposition to combine a modified Dowell's model with the double-2-D model to predict the true leakage inductance of partially-filled transformers at any given frequency. All three conductor types—round, foil, and litz wire—are modeled and analyzed. The quasi-2-D model is further investigated on a variable inductance transformer (VIT) whose winding geometry can be modified mechanically to vary its leakage inductance. With less than 5% error throughout, the semi-analytically evaluated leakage inductances are in excellent agreement with the finite element method (FEM) simulated and experimentally measured leakage inductances.

1. Introduction

Leakage inductance is a critical design element of a transformer in a galvanically isolated power electronic converter. Being the byproduct of the magnetic energy stored in the 3-D space in and around the transformer, its calculation involves the solution to a 3-D problem. Numerical techniques to solve this 3-D problem are available in the form of FEM, which is accurate but computationally inefficient Fouineau et al. (2018); Sharma and Kimball (2021a). On the other hand, multi-objective optimization-based designs of power electronic converters are gaining pace, where cost, efficiency, power density, stability, reliability, etc. are some of the key objectives Garcia-Bediaga et al. (2017); Gu et al. (2022). Therefore, analytical or semi-analytical methods are highly desired that can calculate the leakage inductance swiftly yet accurately Schlesinger and Biela (2021).

In a transformer, the skin effect tends to confine 63% of the total current to an area within one skin depth δ from the outer surface of the conductor when the diameter or thickness of the conductor is greater than 2δ at the switching frequency of the converter. If the winding layers are placed very close to each other, then the proximity effect restricts the current density to an even narrower region. For a given conductor size, these eddy current effects are more pronounced at higher frequencies as δ shrinks further. This non-homogeneous current density reduces the magnetic energy stored in the windings. As a result, the leakage inductance exhibited by a transformer at 1 MHz can be significantly smaller than that at 1 kHz Mogorovic and Dujic (2019). Therefore, it is critical to model the leakage inductance at the specific operating frequency range of the transformer, especially for frequency-controlled resonant converters.

While litz wires with individual strand diameters less than δ may seem quite attractive to annul the eddy current effects in high-frequency, high-power transformers, they are typically much more expensive than single-stranded round wires and are also difficult to manufacture. Consequently, single-stranded round wires are still a preferred choice in many applications. Moreover, with the penetration of wide band-gap devices, the switching frequencies of power converters have reached the MHz region where even litz wires can exhibit skin and proximity effects due to the lack of smaller strand sizes. Hence, both round and Litz wire conductors must be investigated for skin and proximity effects.

The analytical and semi-analytical methods available for calculating the transformer leakage inductance can be broadly classified into either LF or HF models, and either 1-D or 2-D models. In contrast to LF models,

* Corresponding author.
E-mail addresses: asc4v@mst.edu (A. Sharma), kimballjw@mst.edu (J.W. Kimball).

https://doi.org/10.1016/j.pedc.2023.100038
Received 26 January 2023; Received in revised form 1 March 2023; Accepted 9 March 2023
Available online 16 March 2023

Nomenclature

FEM	finite element method
HF	high frequency or frequency-dependent
IW	inside window
LF	low-frequency or frequency-independent
OW	outside window
PEEC	partial element equivalent circuit
TR	transition region
VIT	variable inductance transformer
d_l	partial leakage length
d_w	mean length turn (MLT)
δ	skin depth
Δ	penetration ratio
E_{foil}	stored magnetic energy in a foil
E'	magnetic energy per unit length
E'_{foil}	E' across a foil
E'_{nw}	E' across the interwinding spaces
f	frequency
f_{th}	threshold frequency
g	change in the overlap between winding heights
γ	propagation constant
h	window height
h_c	height of a litz wire bundle
H_r	net magnetic field intensity
h_w	winding height
H_x	radial or x-component of magnetic field intensity
H_y	axial or y-component of magnetic field intensity
I_1	primary current
l	leakage radius
L'	leakage inductance per unit length
L'_{Hx}	L' due to H_x only
L'_{Hy}	L' due to H_y only
L_{lk}	leakage inductance
μ	permeability
μ_0	permeability of free space
n_s	number of litz strand
φ_1	skin effect factor
φ_2	proximity effect factor
r_c	radius of the circular winding leg
r_s	radius of a litz strand
r_w	radius of a round conductor
s	side of a square conductor
σ	conductivity
θ	leakage angle
t_c	thickness of a litz wire bundle
t_s	thickness of a litz strand foil
t_w	thickness of a rectangular foil
w	width of the IW plane
ω	angular frequency

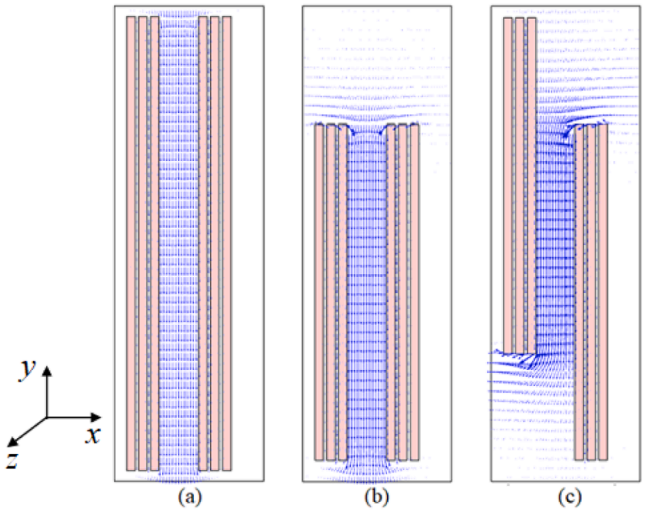

Fig. 1. Magnetic field intensities in the IW plane at 100 kHz: (a) $h_w \approx h$, (b) $h_w < h$ with both windings overlapping each other completely, (c) $h_w < h$ with one of the windings vertically shifted resulting in a reduced overlap.

the HF models account for the eddy current effects in transformer windings, thereby making them suitable for HF transformer designs. While the 1-D models consider only H_y McLyman (2004), the 2-D models consider both H_x and H_y for better accuracy. The magnetic image method is commonly used in 2-D LF models Duppalli and Sudhoff (2017); Eslamian and Vahidi (2012); Fouineau et al. (2018); Gomez and de Leén (2011); Lambert et al. (2013); Margueron et al. (2007a,b); Schlesinger and Biela (2020); Sharma and Kimball (2021a,b); Tan et al. (2016). The closed-form solution of the image method can be obtained either through Fourier expansion of Poisson's and Laplace's equations for the magnetic vector potential Eslamian and Vahidi (2012); Gomez and de Leén (2011); Lambert et al. (2013); Tan et al. (2016) or by using PEEC Magot et al. (2004); Margueron et al. (2007a,b). A comparison of different LF models can be found in Schlesinger and Biela (2021).

Among the LF models, the double-2-D model has drawn a lot of attention lately due to its excellent adaptability to different winding geometries and cores including partially-filled transformers Duppalli and Sudhoff (2017); Eslamian and Vahidi (2012); Fouineau et al. (2018); Gomez and de Leén (2011); Prieto et al. (2003); Schlesinger and Biela (2020); Sharma and Kimball (2021a,b). It calculates the total leakage inductance from the magnetic energy per unit length evaluated across an IW and an OW plane of the transformer. Modeling the two planes is found to be critical for accuracy concerns as the magnetic energy per unit length evaluated across the IW plane is typically higher than its average value around the transformer. Further, instead of using MLT, the improved model in Sharma and Kimball (2021a,b) calculates the depths of the two planes from the average magnetic energy per unit length evaluated across the IW and OW planes.

A 2-D HF model currently does not exist. Dowell pioneered the development of a 1-D model that addresses the eddy current effects in transformer windings Dowell (1966); Villar (2010). Inspired by Dowell's work, Hurley and Wilcox (1994), Wilcox et al. (1988) and Niemela et al. (1989) individually made some remarkable progress in solving the Helmholtz differential equation for the magnetic field intensity in the IW plane of the transformer to compute the frequency-dependent leakage inductance. These models are derived using the following key assumptions:

(1) stored magnetic energy inside the core is zero,
(2) winding cross-sections are frequency-dependent while non-winding spaces are frequency-independent regions,
(3) H_x is zero throughout the IW plane,
(4) H_r $(= H_y)$ depends on the position of the winding layers along x-axis only,
(5) variation of H_r along y-axis is zero,

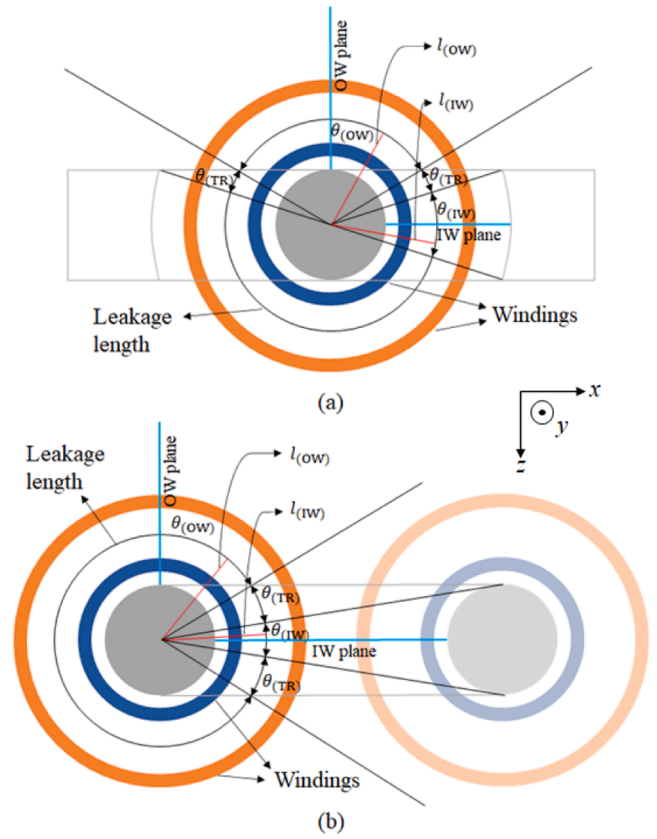

Fig. 2. Double-2-D model: (a) shell-type transformer, (b) core-type transformer Sharma and Kimball (2021a).

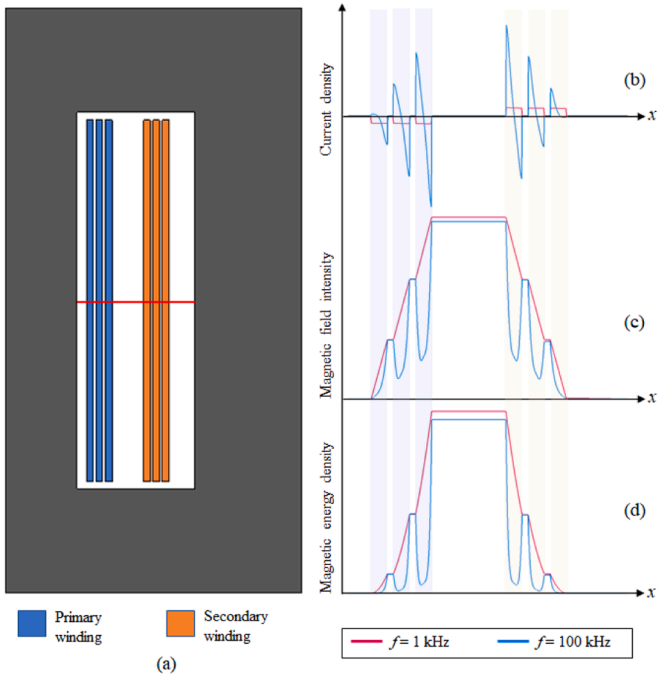

Fig. 3. (a) 2-D axisymmetric transformer cross-section with three primary and three secondary winding layers. Also shown are the corresponding FEM plots across the marked cut-line at different frequencies: (b) current density, (c) magnetic field intensity, (d) magnetic energy density.

(6) variation of magnetic energy per unit length around the transformer is zero.

Assumptions (3)–(6) limit the scope of these models to fully-filled transformers where $h_w \approx h$, as represented in Fig. 1(a), so that H_x is negligible. Although Bahmani and Thiringer (2015), Ouyang et al. (2015) and Kaijia et al. (2019) made some improvements to Hurley's model, the assumptions remain unchanged. Ouyang et al. (2019) further modeled the radial magnetic fields in planar transformers and developed a 1-D model that ignores the axial fields completely. Mogorovic and Dujic (2017, 2019) developed a 1-D model for litz wire transformers, where each layer of litz wire is assumed as multiple layers of litz strands that compose the wire. Recently, a new litz wire model was proposed in Zhang et al. (2020), which accounts for the eddy current effects in individual strands. Rogowski's factor and other porosity factors were suggested in Guo et al. (2022); Mogorovic and Dujic (2017, 2019); Villar (2010) for winding heights shorter than window height, but the position of the foil along y-axis still remains unaccounted for.

In a partially-filled transformer with a smaller fill-factor, assumption (3) is not valid because the fringing magnetic fields around the edges of the windings contribute significantly to H_x Schlesinger and Biela (2021). Fig. 1(b) illustrates this point further. Moreover, in a VIT Sharma and Kimball (2021a,b), a decrease in the overlap between the two winding heights increases the effective leakage inductance due to an increase in H_x, as indicated by Fig. 1(c). As such, assumption (4) makes the existing HF models completely insensitive to any variations in overlap, thus leading to exponential errors. Furthermore, the magnetic energy per unit length across the IW plane is typically higher than that across the OW plane. As such, assumption (6) can overestimate the net leakage inductance of the VIT considerably. In summary, an HF model that can accurately predict the frequency-dependent leakage inductance of partially-filled transformers including VITs is still missing in the literature.

This paper proposes a hybrid model that overcomes the above challenges to predict the true leakage inductance of a partially-filled transformer at any given frequency. This quasi-2-D model uses superposition to combine a modified HF Dowell's model with the LF double-2-D model. The proposed model is used to meet three main objectives:

1. evaluating the frequency-dependent leakage inductance of a transformer that is wound with round conductors and has a winding height significantly smaller than the window height,
2. evaluating the frequency-dependent leakage inductance of a transformer that is loosely wound with litz wires along the winding height,
3. evaluating the frequency-dependent leakage inductance of a VIT at different overlaps.

The paper begins with a quick overview of the double-2-D and Dowell's 1-D models for background before diving deep into the challenging winding geometry of a VIT. Then, the hybrid model is proposed and the geometrical modelings of different conductor types are explained. Results fulfilling the three main objectives are presented and further discussed. The paper finally ends with a concluding remark.

2. Double-2-D model

Evaluation of leakage inductance is inherently a 3-D problem. The double-2-D model reduces this 3-D problem into two separate 2-D problems, wherein E' is evaluated across two planes—the IW plane and the OW plane—using the fundamental equation Sharma and Kimball (2021a,b),

$$E' = \frac{\mu_0}{2} \int \int H_r^2(x,y)\, dx\, dy \tag{1}$$

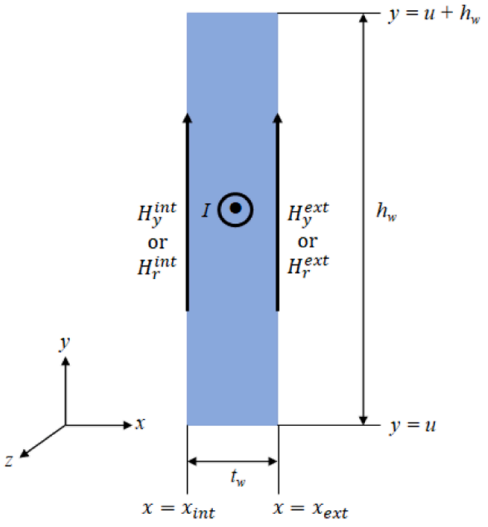

Fig. 4. Rectangular foil carrying a net current I.

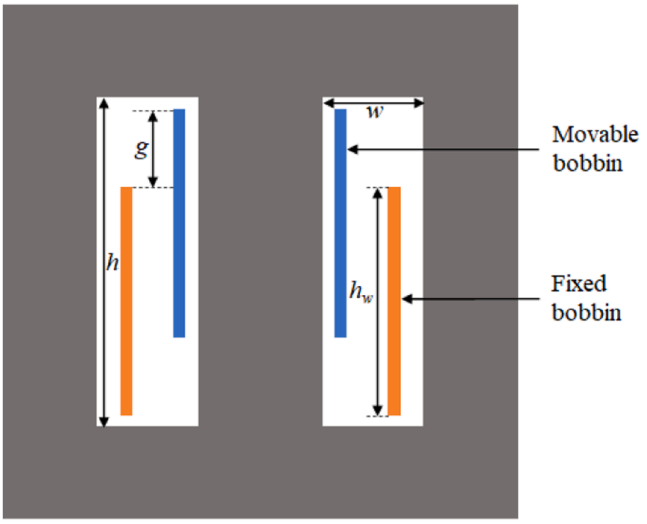

Fig. 5. 2-D model of a VIT.

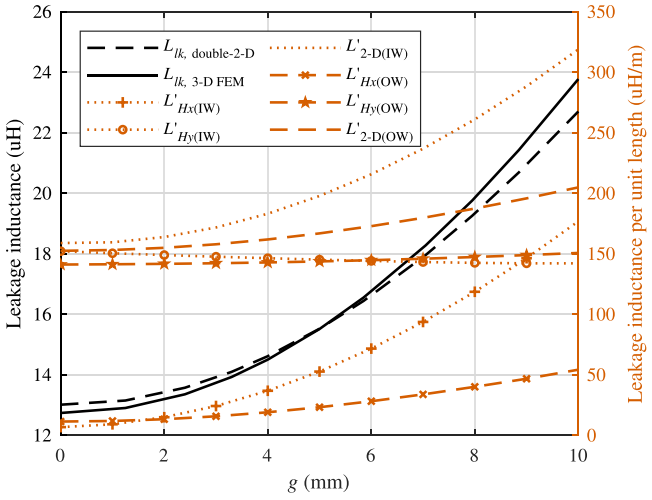

Fig. 6. Variable LF leakage inductance of a VIT Sharma and Kimball (2021a).

$$H_r = \sqrt{H_x^2 + H_y^2}$$

Fig. 2 illustrates the concept of the double-2-D model Sharma and Kimball (2021a,b). The general form of this model is given by,

$$L_{lk,\text{double-2-D}} = s_c\left(L'_{(\text{IW})}d_{l(\text{IW})} + L'_{(\text{OW})}d_{l(\text{OW})}\right) \tag{2}$$

$$s_c = \begin{cases} 1, & \text{core-type transformer} \\ 2, & \text{shell-type transformer} \end{cases}$$

The improved double-2-D model averages E' across each plane to find the corresponding l, which is then used to find d_l. Please see Appendix A for more details. Finally, the leakage inductance can be obtained by using (2). The underlying assumptions are that L' evaluated across a plane is uniform in that region, and the stored magnetic energy inside the core is zero.

The improved double-2-D model uses the magnetic image method to calculate the magnetic energy per unit length across the two planes. As per the image method, the transformer core acts as a reflective medium for any current-carrying conductor placed near it. The IW plane that is bounded by the core on all four sides results in an infinite series of image conductors, while the OW plane that is bounded by the core on one side only results in a single image conductor. Hence, the accuracy of the double-2-D model depends on the number of image layers being considered in the IW plane. Sharma and Kimball (2021a) suggests modeling the nearest two image layers as a good choice.

3. Dowell's 1-D model

Fig. 3 shows a 2-D axisymmetric transformer cross-section with multiple rectangular foil layers that constitute the primary and secondary windings. It also shows the FEM simulated current density, magnetic field intensity, and magnetic energy density at different frequencies across the horizontal cut-line that bisects the IW plane. At 1 kHz, the current density is uniform; so the corresponding change in magnetic field intensity is also linear across the foil cross-sections. But at 100 kHz, the skin and proximity effects cause a non-uniform current density that further leads to a non-linear field intensity across the foil cross-sections. These effects can be related to δ, which is a measure of the current density across the cross-section of the conductor, given by

$$\delta = \sqrt{\frac{1}{\pi\mu f\sigma}} \tag{3}$$

Fig. 3 also suggests that the eddy current effects influence the magnetic energy densities in the foil cross-sections only, not so much in the non-winding spaces because the net current is conserved Villar (2010). Hence, the winding cross-sections can be assumed as frequency-dependent regions while the non-winding spaces as frequency-independent regions.

Dowell investigated the orthogonality between the skin and proximity effects and derived a simple 1-D model from the phasor integral of the 1-D Helmholtz differential equation for H_y across the IW plane of the transformer. For the rectangular foil shown in Fig. 4, the frequency-dependent magnetic energy per unit length stored in it can be calculated using Villar (2010),

$$E_{\text{foil}} = \frac{\mu_0 d_w h_w \delta}{4}\left(\left(H_y^{ext} + H_y^{int}\right)^2\varphi_1 - 2H_y^{ext}H_y^{int}\varphi_2\right) \tag{4}$$

$$\varphi_1 = \frac{\sinh(2\Delta) - \sin(2\Delta)}{\cosh(2\Delta) - \cos(2\Delta)},$$

$$\varphi_2 = \frac{\sinh(\Delta) - \sin(\Delta)}{\cosh(\Delta) - \cos(\Delta)}$$

where H_y^{int} and H_y^{ext} are the internal and external magnetic field in-

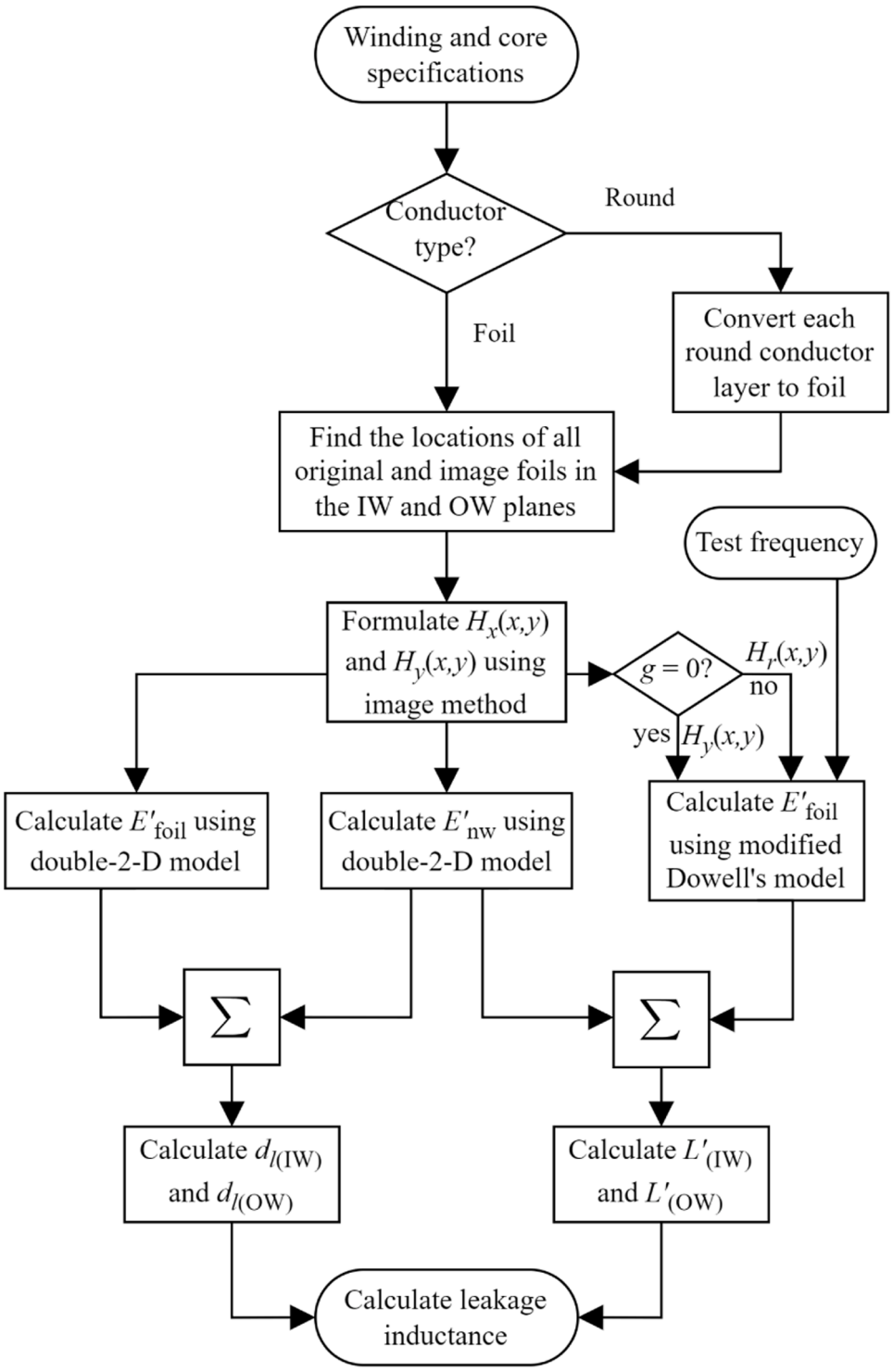

Fig. 7. Flowchart of the proposed hybrid model.

tensities in y-direction evaluated at $x = int$ and $x = ext$ respectively, and $\Delta = t_w/\delta$. The mathematical derivation of (4) is given in Appendix B. A module integral-based approach to solve the Helmholtz differential equation can be found in Dang et al. (2022). Overall, Dowell's model performs fairly well when the foils are of equal height $h_w \approx h$, as indicated in Fig. 3(a), so that H_x due to the primary and secondary conductors nearly cancel each other, and the net magnetic field intensity $H_r \approx H_y$.

4. Variable inductance transformer

A VIT is a partially-filled transformer that allows users to vary its leakage inductance mechanically. It was first introduced in Sharma and Kimball (2021b). In a VIT, the winding height is significantly smaller than the window height. By using a linear actuator, one of the windings can be moved along the core leg. This reduces the overlap between the two winding heights, thereby increasing the leakage inductance. Fig. 5 shows the 2-D model of a VIT. The improved double-2-D model proved very effective in evaluating the variable LF leakage inductance of a VIT.

Fig. 6 plots the variable LF leakage inductance as a function of g. A maximum error of only 4.5% was observed at $g = 10$ mm when the nearest three image layers (48 images) were considered in the IW plane Sharma and Kimball (2021a).

In Fig. 6, $L'_{Hx} + L'_{Hy} = L'$. This figure shows that an increase in g has a negligible effect on H_y in either plan. Instead, the increase in leakage inductance with g is an outcome of the increase in H_x only, if partial leakage lengths are assumed constant. The existing HF models being 1-D ignore H_x completely; hence using such models in a VIT result in a flat horizontal curve for the evaluated leakage inductance at different g values. Moreover, the increase in L'_{Hx} with g is much higher across the IW plane than that across the OW plane, i.e. $L'_{(\mathrm{IW})} > L'_{(\mathrm{OW})}$ for $g > 0$ mm. As such, analyzing the IW plane only with an existing HF model can overestimate the total leakage inductance considerably.

5. Proposed hybrid model

In this paper, a semi-analytical hybrid model is proposed for evaluating the frequency-dependent leakage inductance of partially-filled transformers including VITs. This hybrid model is built on the double-2-D model platform presented in (2) and uses superposition to combine a modified Dowell's model with the double-2-D model Sharma and Kimball (2022). The modified Dowell's model calculates the magnetic energy per unit length from the frequency-dependent winding cross-sections, while the double-2-D model calculates the same from the frequency-independent non-winding spaces. The proposed model uses the following basic assumptions:

(1) stored magnetic energy inside the core is zero,
(2) winding cross-sections are frequency-dependent and non-winding spaces are frequency-independent regions,
(3) magnetic energy per unit length across a plane is uniform along its leakage length.

For simplicity, all primary and secondary foils are assumed to be of equal height $h_w < h$. The modified Dowell's model calculates the magnetic energy per unit length across the foil in Fig. 4 using,

$$E'_{\mathrm{foil}} = \frac{\mu_0 \delta}{4} \int_u^{u+h_w} \left(\left(H_r^{ext}(y) + H_r^{int}(y)\right)^2 \varphi_1 - 2H_r^{ext}(y) H_r^{int}(y) \varphi_2 \right) dy \tag{5}$$

where u is the y-coordinate of the bottom edge of the concerned foil. (5) can be adapted for two different partially-filled transformer winding geometries:

(i) $g = 0$, as shown in Fig. 1(b), where H_x can be assumed negligible across the foil cross-section so that $H_r(y) = H_y(y)$, and
(ii) $g \neq 0$, as shown in Fig. 1(c), where H_x is no longer negligible across the foil cross-section. However, resolving the convoluted 2-D Helmholtz differential equation with the correct boundary conditions will necessitate evaluating H_x at the top and bottom edges of the foil Gerling (2009). The solution becomes computationally more intensive particularly when the foil consists of several round conductors arranged in a single layer, where H_x must be evaluated at the top and bottom edges of each conductor. In order to reduce the computational burden without introducing a substantial error to the calculated leakage inductance, a simplification is made here, where $H_r(y) = \sqrt{(H_x^2(y) + H_y^2(y)}$. This simplification is validated in the results section through FEM simulations and experimentation.

$H_r^{int}(y)$ and $H_r^{ext}(y)$ in (5) can be obtained from the double-2-D model by evaluating $H_r(x, y)$ at $x = int$ and $x = ext$, respectively. The integration in y-direction takes care of any deviations in $H_r(y)$ along the height of the foil. (5) also permits the use of partial leakage length as the depth of the concerned plane for better accuracy.

The flowchart of the hybrid model is shown in Fig. 7. First, each layer of round conductors is converted to a foil of thickness as prescribed in Section 6. Next, the precise locations of the foils are determined, and H_x and H_y due to each foil are modeled using the equations given in Appendix C. Then, the image method is used to model the net H_x and H_y due to all original and image foils in both IW and OW planes. Since non-winding spaces are frequency-independent regions, (1) is used to compute E'_{nw}. Next, the frequency-dependent E'_{foil} is determined across each foil using (5). Then, using superposition, the net magnetic energy per unit length across a plane at any given frequency can be calculated using,

$$E' = E'_{\mathrm{nw}} + \sum_{\mathrm{all}} E'_{\mathrm{foil}}. \tag{6}$$

E' is scaled by $2/I_1^2$ to compute L' across each plane. Since a change in frequency barely changes the partial leakage length d_l, the frequency-independent E'_{foil} is evaluated across each foil using (1), which is then added to E'_{nw} to find the frequency-independent E' across each plane. This E' is used to find d_l across a plane using the equations given in Appendix A. Finally, the frequency-dependent leakage inductance of the transformer can be calculated using (2).

6. Conductor types

6.1. Round and foil conductors

Round and foil conductors are frequently used in transformer windings. Mathematical formulations for calculating the magnetic field intensity in x- and y-directions at any given point in and around a round or a foil conductor are given in Sharma and Kimball (2021a). Since a round conductor is difficult to model in the Cartesian coordinate system, it may be favorable to convert it into a square conductor of an equivalent area such that $s = r_w\sqrt{\pi}$. However, if the transformer is wound with hundreds of round conductors that are densely packed along the winding height, it may be convenient to model each layer of round conductors as a rectangular foil. The accuracy is higher when the assumed thickness of the foil $t_w = r_w\sqrt{\pi}$ Sharma and Kimball (2021a). Appendix C gives the formulations for the magnetic field intensities due to a current-carrying foil. For a transformer wound with round conductors where $h_w < h$, the LF double-2-D model presented an error as small as 0.09% when the round conductors were assumed as square conductors of equivalent area, and 0.46% when a layer of round conductors was assumed as a rectangular foil of thickness t_w, both considering the nearest two image layers (24 images) in the IW plane Sharma and Kimball (2021a).

6.2. Litz wire

Litz wire is a multi-strand wire that is specifically designed to minimize skin and proximity effects. To do so, $r_s < \delta$ must be selected. The number of strands n_s that make a litz wire bundle depends on the ampacity of the strand as well as the rated transformer current Sullivan (1999). In a precisely designed litz wire transformer, the skin and proximity effects are negligible. As such, a single litz wire bundle can be assumed as a round conductor having a radius $r_w = r_s\sqrt{n_s}$. If the wires are densely packed along the winding height, then the double-2-D model can evaluate the frequency-independent leakage inductance if each layer of litz wire is converted to a foil of thickness $t_w = r_s\sqrt{\pi n_s}$.

At frequencies near and above f_{th} when $r_s = \delta$, the skin and proximity effects become visible across the cross-sections of each litz strand, thereby leading to a smaller leakage inductance than that at a lower frequency. If the wires are densely packed along the winding height, then a layer of litz wires can be approximated as a foil having a thickness t_w, similar to Mogorovic and Dujic (2017). The magnetic energies per

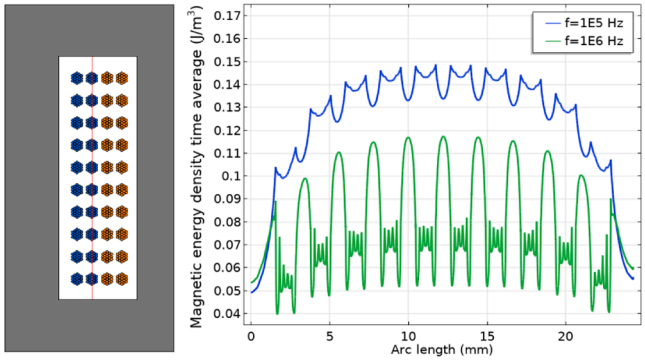

Fig. 8. IW cross-section of the litz wire transformer with the associated magnetic energy densities at 100 kHz and 1 MHz across the marked cut-line.

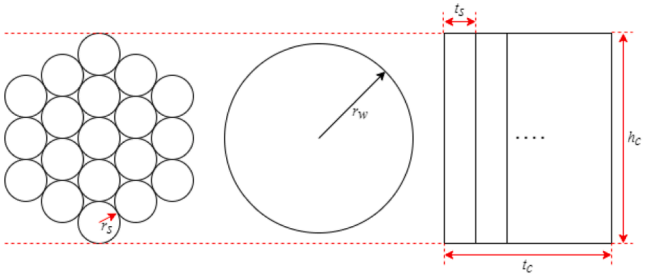

Fig. 9. Geometrical models of litz wire: (a) litz wire with 19 strands ($p = 3$), (b) round conductor approximation, and (c) rectangular conductor approximation.

Table 1
Transformer I specifications.

Parameter	Value
Turns ratio	1:1
Conductor type, size	Round, AWG 19
Number of turns per layer	30
Number of layers per winding	3
Core geometry	EC 70
Window height	45.50 mm
Winding height	31.50 mm
External diameter of the movable bobbin	19 mm
External diameter of the fixed bobbin	33 mm
Insulation gap between layers	0.20 mm
Gap between turns along winding height	0.14 mm
Fill-factor	19.04%
Maximum travel of the movable bobbin	11 mm
Test frequency range	1–200 kHz
Air cube	80^3 mm^3

unit length across the non-winding spaces can be calculated using the double-2-D model, while those across the foils can be calculated using the modified Dowell's model in (5), where the penetration ratio for the current in an individual litz strand must be considered for accuracy. Conceptually, a single foil of thickness t_w can be approximated as $k_c = t_w / t_s$ number of thin foils of thickness $t_s = r_s\sqrt{\pi}$ and height h_w stacked tightly without any insulation gap between them.

However, the litz wire transformer assumed for investigating the proposed hybrid model is loosely wound along the winding height, as shown in Fig. 8. In such a case, the magnetic energy per unit length across the non-winding space between two consecutive bundles can be significantly higher than that across the bundle at frequencies above f_{th}. So, converting a layer of litz wires into a foil can lead to an erroneous result. In this paper, each litz wire bundle is modeled individually for higher accuracy. For a hexagonal $p-$ layered bundle, like the one shown in Fig. 9, $n_s = 3p^2 - 3p + 1$, where $p = 1, 2, 3, \ldots$. To use the hybrid

Table 2
Transformer II specifications.

Parameter	Value
Turns ratio	1:1
Number of litz strands	19
Size of each litz strand	AWG 30
Number of turns per layer	10
Number of layers per winding	2
Core geometry	ETD 34
Window height	24.30 mm
Winding height	20.90 mm
External diameter of the bobbin	13.60 mm
Insulation gap between layers	0.20 mm
Insulation gap between windings	0.25 mm
Gap between turns along winding height	0.95 mm
Fill-factor	20.34%
Test frequency range	1 kHz–1 MHz
Air cube	50^3 mm^3

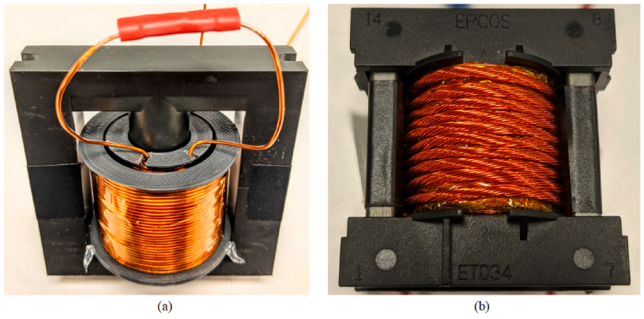

Fig. 10. Experimental prototypes: (a) Transformer I, and (b) Transformer II.

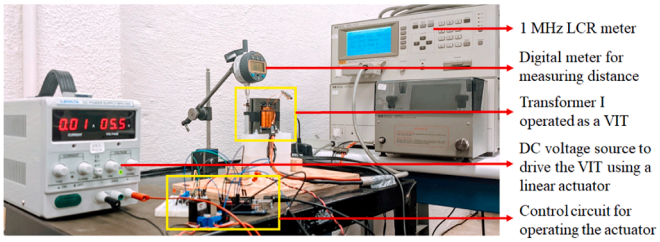

Fig. 11. Experimental measurement setup with the VIT.

model, each bundle is converted to a rectangular conductor having a thickness $t_c = 2r_s\{1 + 2(p-1)\sin(\pi/3)\}$ and height $h_c = 2r_s(2p - 1)$, as illustrated in Fig. 9. The magnetic energy per unit length across the non-winding spaces is calculated using the double-2-D model. For calculating the same across the rectangular conductors, the penetration ratio of current in an individual litz strand is considered in (5), which is $\Delta = t_s/\delta$ and $t_s = r_s\sqrt{\pi}$. Finally, the magnetic energy per unit length across one complete bundle is obtained by scaling the above results by the factor $k_r = \lceil t_c / t_s \rceil$.

7. Results

The proposed hybrid model is formulated to meet the three main objectives stated in section I, and thus to demonstrate the applicability of the model to any transformer winding geometry. Two partially-filled transformers with different winding and core geometries are considered. Transformer I is wound with round conductors and has a winding height significantly smaller than the window height. It also functions as a VIT. Transformer II is loosely wound with multi-strand litz wires along the winding height. The specifications of the two transformers are provided in Tables 1 and 2. Since the net primary leakage inductance is a scalar

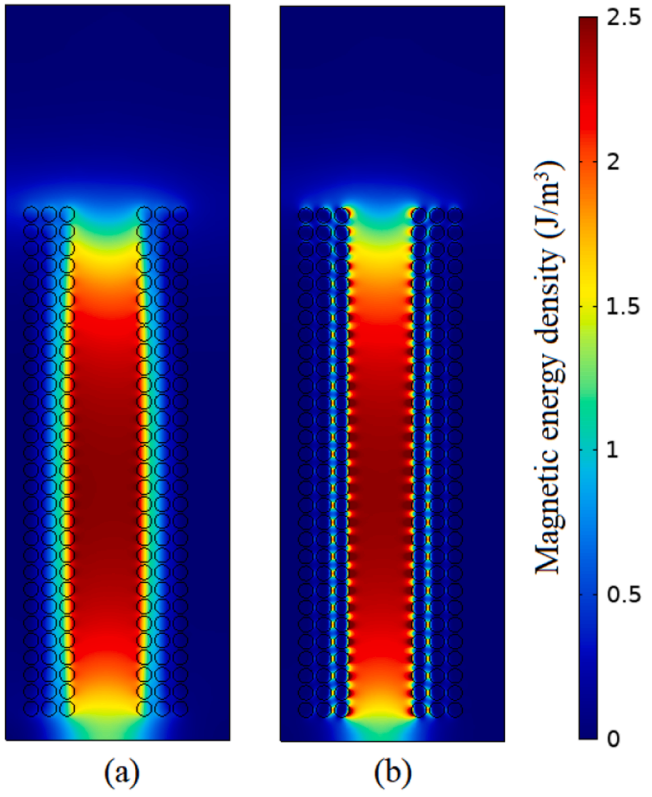

Fig. 12. Magnetic energy densities across the IW plane of Transformer I: (a) 1 kHz, and (b) 200 kHz.

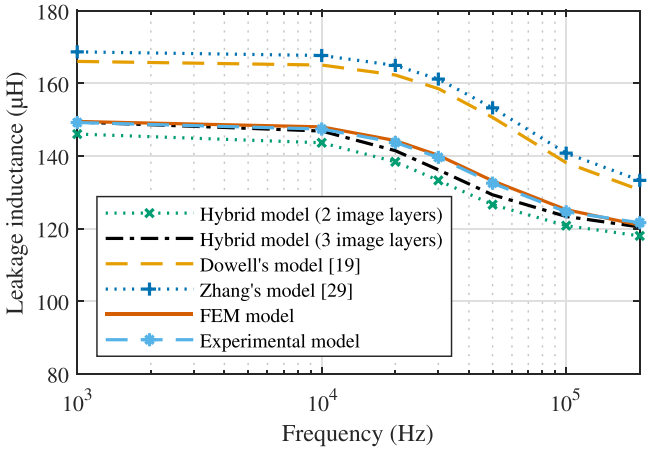

Fig. 13. Leakage inductances of Transformer I.

multiple (square of the turns ratio) of the net secondary leakage inductance, only unity turns ratio transformers are modeled in this paper to avoid any redundant results.

Fig. 10 shows the experimental prototypes of the two transformers, while Fig. 11 demonstrates the measurement setup with the VIT. MATLAB R2019a is used to calculate all semi-analytical leakage inductances. The 2-D FEM results are obtained using COMSOL Multiphysics 5.5, where the IW and OW planes of the two transformers are modeled individually to find the leakage inductance per unit length across them as well as the corresponding partial leakage lengths. Finally, the leakage inductances are calculated using the double-2-D model presented in (2). These results are considered the standards for determining the accuracy of the proposed model. Results fulfilling the three stated objectives are presented in the following subsections.

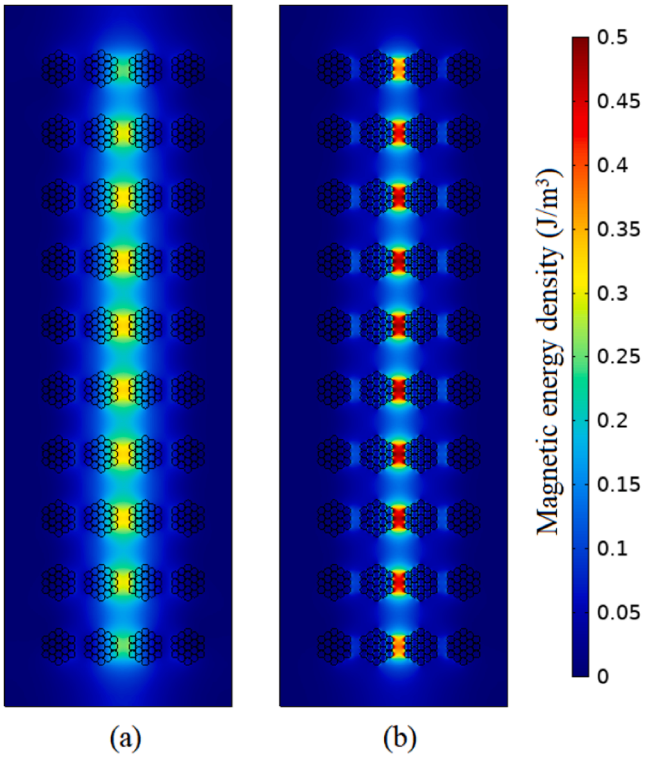

Fig. 14. Magnetic energy densities across the IW plane of Transformer II: (a) 100 kHz, and (b) 1 MHz.

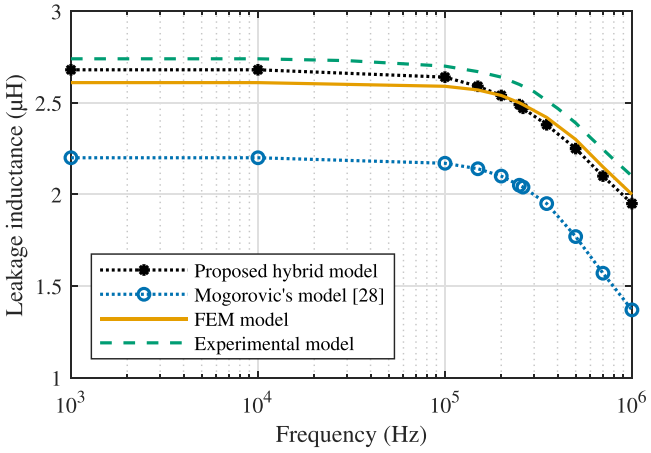

Fig. 15. Leakage inductances of Transformer II.

7.1. *Transformer I: round conductor* ($g = 0$)

The primary and secondary windings of Transformer I are wound with a single strand of round conductors that has a threshold frequency of 20.4 kHz. Although Transformer I can be used as a VIT, results presented in this subsection pertain to the case when $g = 0$ so that $H_r(y)$ in (5) can be replaced with $H_y(y)$. Fig. 12 plots the FEM simulated magnetic energy densities across the IW plane at 1 and 200 kHz. A visual comparison between the two plots verifies the reduction in magnetic energy density across the winding cross-sections at 200 kHz due to skin and proximity effects. Here, the maximum test frequency is limited to 200 kHz so that the influence of the interwinding capacitance on the measured leakage inductance can be avoided.

Fig. 13 plots the leakage inductances of Transformer I as a function of frequency obtained from the hybrid, FEM, and experimental models. For

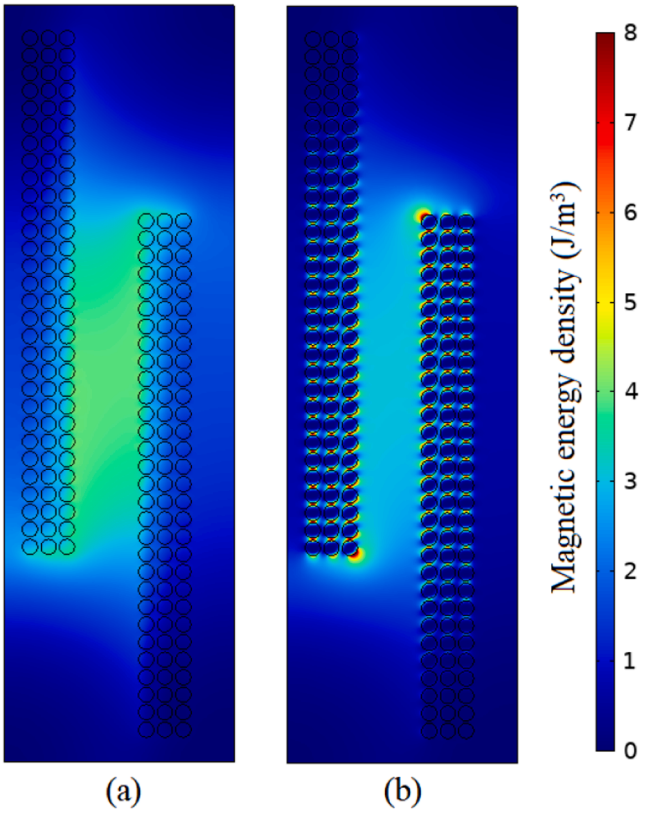

Fig. 16. Magnetic energy densities across the IW plane of Transformer I operated as a VIT at $g = 11$ mm: (a) 1 kHz, and (b) 200 kHz.

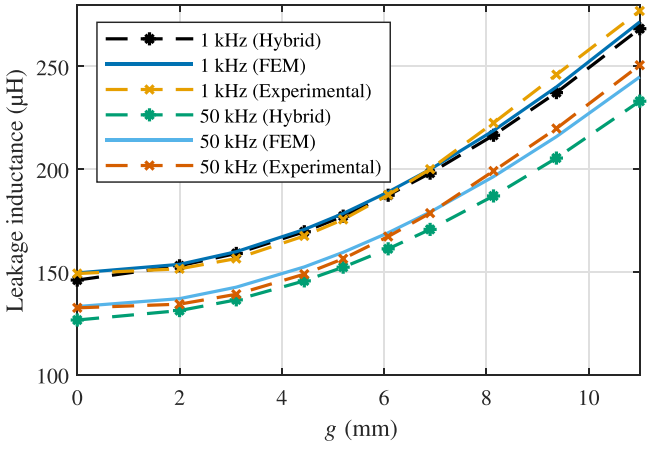

Fig. 17. Variation of leakage inductance with g at 1 and 50 kHz.

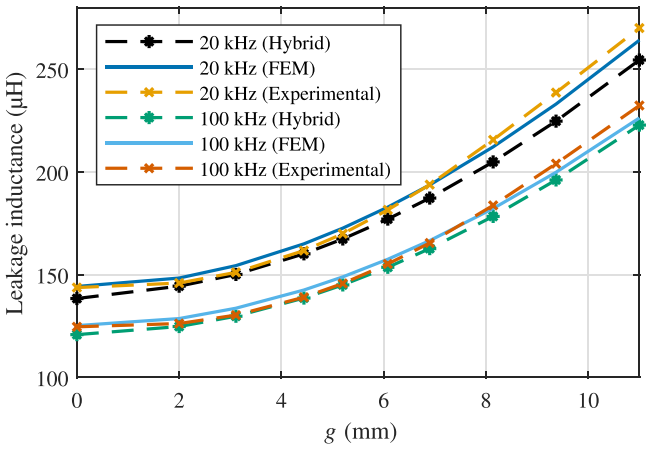

Fig. 18. Variation of leakage inductance with g at 20 and 100 kHz.

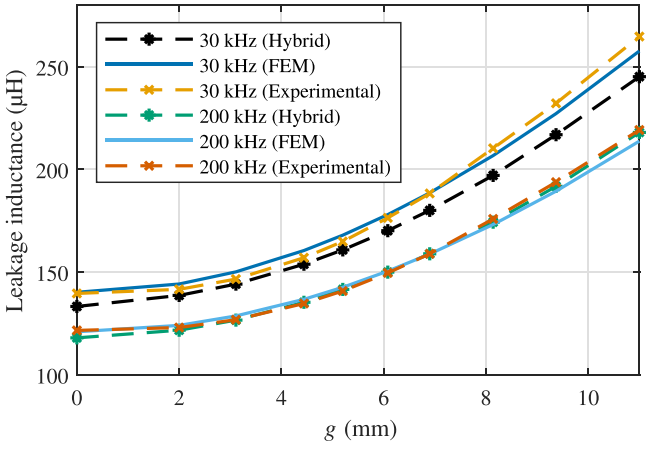

Fig. 19. Variation of leakage inductance with g at 30 and 200 kHz.

Table 3
Errors for transformer I at $g = 11$ mm considering different number of image layers in the IW plane.

Frequency (kHz)	Number of image layers	Leakage inductance (μH)	Error (%)	Computation time (p.u.)
30	1	240.95	6.49	1
	2	245.16	4.86	3.5
	3	259.93	–0.88	7.5
	4	256.49	0.46	14.1
50	1	229.30	6.37	1
	2	233.08	4.82	3.5
	3	246.90	–0.82	7.5
	4	243.64	0.51	14.1

comparison, it also plots the leakage inductances evaluated using Dowell's Villar (2010) and Zhang's Zhang et al. (2020) 1-D models, both considering porosity factors. Both Dowell's and Zhang's models overestimate the leakage inductances throughout the entire test frequency range. While Dowell's 1-D model shows a peak error of 13.12% at 30 kHz, Zhang's model presents a peak error of 15.09% at 50 kHz. In contrast, with the hybrid model, a peak error of only 4.93% is observed at 50 kHz if the nearest two image layers are considered in the IW plane. The errors are seen to be higher between 30 and 50 kHz where the slope of the decreasing leakage inductance is at its peak. These errors can be reduced by modeling the third image layer which decreases the peak error at 50 kHz to just 2.89%. Hence, it can be concluded that the proposed hybrid model can prove very effective in calculating the frequency-dependent leakage inductance of partially-filled transformers wound with round conductors, thus fulfilling the first main objective. Additionally, the experimental leakage inductance curve completely overlaps with its FEM counterpart throughout the test frequency range, thereby highlighting the precise construction of the experimental prototype. Overall, the leakage inductance of the experimental prototype dropped by 18.5% between 1 and 200 kHz.

7.2. *Transformer II: litz wire* ($g = 0$)

The primary and secondary windings of Transformer II are loosely wound with two layers of 19-strand litz wires. The threshold frequency of the litz strand is 261.4 kHz. The FEM-generated magnetic energy

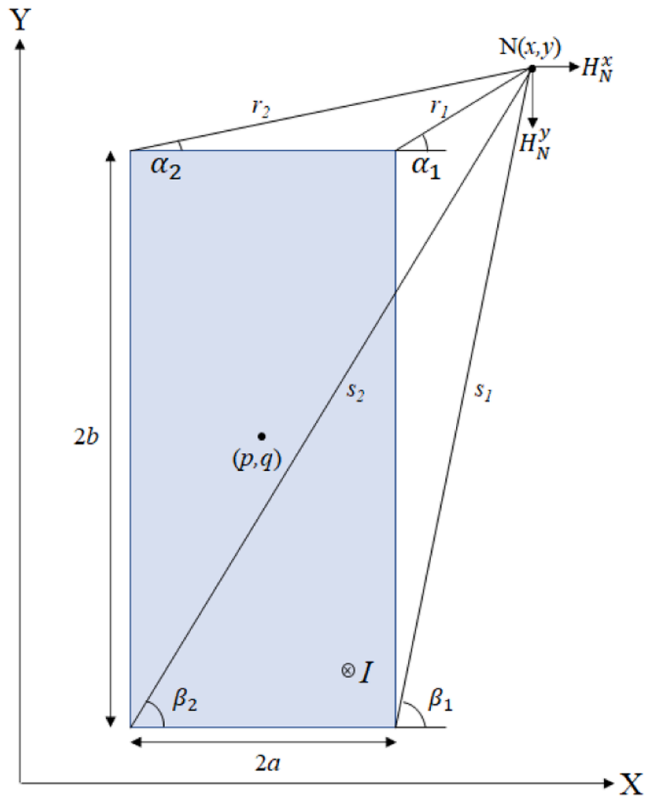

Fig. 20. Rectangular foil carrying a current *I*.

densities across the IW plane of the transformer at 100 kHz and 1 MHz are plotted in Fig. 14. Please note that the insulation thickness of the enameled litz strands is not taken into account. Besides, in a practical transformer, the layout of the strands will vary from the ideal layout shown in Fig. 9 due to the twisting inherent to litz construction.

Fig. 15 plots the leakage inductances of Transformer II as a function of frequency obtained from the hybrid, FEM, and experimental models. In the case of hybrid model, only the nearest two image layers are considered in the IW plane. For comparison, it also plots the leakage inductances evaluated using Mogorovic's 1-D model for litz wires that considers Rogowski's factor Mogorovic and Dujic (2017, 2019). Mogorovic's model underestimates the leakage inductances by more than 15% throughout the test frequency range. The peak error is noticed at 1 MHz, which is 31.5%. The prime reason behind this large error is found to be the magnetic energy across the non-winding spaces between successive turns within a layer that is ignored by modeling the layer as a foil. On the other hand, the leakage inductances calculated using the hybrid model concur very well with the FEM and experimental results leading to a peak error of only 2.68% observed at 1 and 10 kHz, which are below f_{th}. This fulfills the second main objective of the paper. Between 1 kHz and 1 MHz, the leakage inductance of the experimental prototype dropped by 23.4%.

7.3. *Variable inductance transformer* ($g \neq 0$)

Having a winding height shorter than the window height makes Transformer I utilizable as a VIT. Although either bobbin may be used as the movable one, it is recommended to use the narrower one for mechanical reasons, as indicated in Fig. 5. Here, the maximum travel of the movable bobbin is limited to 11 mm, and the complete experimental setup with the VIT, linear actuator, 1 MHz LCR meter, and Arduino-based control circuitry is already presented in Fig. 11. Only the nearest two image layers are considered in the IW plane for evaluating the semi-analytical leakage inductances. Fig. 16 plots the magnetic energy densities across the IW plane of the VIT at 1 and 200 kHz obtained from the FEM model at $g = 11$ mm. A visual inspection between the density plots in Figs. 12 and 16 suggests the increase in magnetic energy with g as well as its decrease with frequency.

Figs. 17–19 plots the semi-analytically evaluated, FEM simulated, and experimentally measured leakage inductances for the full range of overlap at different frequencies. These plots reiterate the fact that the effective leakage inductance of a VIT increases with g while it decreases with frequency. In fact, the leakage inductance at $g = 11$ mm is about 80% higher than that at $g = 0$ mm across all frequencies. The existing HF models cannot evaluate this increase in frequency-dependent leakage inductance with g and thus yield a constant leakage inductance at all overlaps due to assumptions (3) and (4) stated in section I, thereby resulting in an error as high as 80% at $g = 11$ mm.

Figs. 17–19 indicate that the FEM and the experimental leakage inductance curves nearly overlap each other at all frequencies. However, a small error ranging between 3.86 and 4.93% is observed between the semi-analytical and FEM curves at 30 and 50 kHz. When compared to Fig. 13 that plots the frequency-dependent leakage inductance of the same Transformer I at $g = 0$ mm, 30–50 kHz is the frequency range where the error and the slope of the decreasing leakage inductance are maximum. These errors can be further improved by modeling the third image layer in the IW plane, as indicated by Table 3. Nevertheless, the peak error is still observed at $g = 0$ mm. An error smaller than the peak error at $g > 0$ mm justifies the simplification made in (5) for winding geometries where $g \neq 0$. Furthermore, these errors decrease with frequency and become negligible at 100 and 200 kHz. Hence, it can be concurred that the proposed hybrid model can calculate the variable frequency-dependent leakage inductance of a VIT with sufficient accuracy, thus fulfilling the third and final objective of the paper.

8. Discussion

The hybrid model proposed in this paper uses superposition to combine a modified Dowell's model with the double-2-D model, thus making it a quasi-2-D model. In contrast to the existing HF models, the proposed model accounts for the actual positions of all winding layers in both the IW and OW planes of the transformer. Secondly, it accounts for both the radial and axial components of magnetic field intensity in the non-winding spaces. These two considerations make the hybrid model naturally more promising for any partially-filled transformer. Such winding geometries are becoming increasingly popular in isolated power converters that utilize the leakage inductance of the transformer to meet the desired series inductance for efficient power conversion. The possibilities of transformer winding geometries are truly immense, which makes the hybrid model even more attractive. Needless to say, the model can also be extended to transformers carrying multi-layer interleaved windings. Although the model is developed keeping in mind the challenging winding geometry of partially-filled transformers, it can certainly be applied to fully-filled transformers.

Built on the double-2-D platform, the accuracy of the hybrid model depends on the number of image layers being considered in the IW plane. Table 3 presents the errors for Transformer I at $g = 11$ mm, and at 30 and 50 kHz where the errors are found to be typically larger. While a higher number of image layers may seem very attractive for better accuracy, it also adds to the total computation time. Thus, selecting this number involves a trade-off. With the nearest two image layers, the peak error was found to be less than 5% for both Transformers I and II. Therefore, it is recommended to model the nearest two image layers for an optimal balance between computation time and accuracy.

Here, the hybrid model is formulated very comprehensively using fewer assumptions than the existing HF models to demonstrate its applicability to any conductor type and winding geometry. Nonetheless, it is capable of undergoing many simplifications depending on the winding geometry and conductor type to meet the desired computational efficiency. Therefore, the proposed hybrid model can be very

useful in multi-objective optimization-based designs of power electronic converters employing transformers with integrated magnetics. It may also be extended to planar transformers. However, special attention must be paid to all geometrical dimensions, since planar transformer windings typically have a larger width-to-height aspect ratio of the conductor cross-section when compared to traditional transformer windings.

9. Conclusion

In this paper, a hybrid model is proposed for calculating the frequency-dependent leakage inductance of partially-filled transformers. This quasi-2-D model uses fewer assumptions than the existing 1-D models and combines the evergreen Dowell's 1-D model with the versatile double-2-D model through superposition. A modified Dowell's model calculates the leakage inductance contributions from the frequency-dependent winding cross-sections, while the double-2-D model calculates the same from the frequency-independent non-winding spaces. Results verify the efficacy of the hybrid model in partially-filled transformers including VITs wound with round, rectangular, and litz wires. With all errors being less than 5%, it is recommended to model the nearest two image layers in the winding window for a perfect balance between computation time and accuracy. Although formulated very comprehensively, the hybrid model is capable of undergoing the simplifications needed to meet the desired computational efficiency. Therefore, the hybrid model can serve as an effective tool in multi-objective optimization-based designs of isolated power converters employing high-frequency transformers with integrated magnetics.

Declaration of Competing Interest

The authors declare that they have no known competing financial interests or personal relationships that could have appeared to influence the work reported in this paper

Data availability

Data will be made available on request.

Acknowledgments

This material is based upon work supported by the Department of Energy Vehicle Technologies Office under Award Number DE-EE0008449. This manuscript was prepared as an account of work sponsored by an agency of the United States Government. Neither the United States Government nor any agency thereof, nor any of their employees, makes any warranty, express or implied, or assumes any legal liability or responsibility for the accuracy, completeness, or usefulness of any information, apparatus, product, or process disclosed, or represents that its use would not infringe privately owned rights. Reference herein to any specific commercial product, process, or service by trade name, trademark, manufacturer, or otherwise does not necessarily constitute or imply its endorsement, recommendation, or favoring by the United States Government or any agency thereof. The views and opinions of authors expressed herein do not necessarily state or reflect those of the United States Government or any agency thereof.

Appendix A. Calculation of partial leakage lengths in double 2-D model Sharma and Kimball (2021a)

In Fig. 2(a), the energy-weighted leakage radius l for the IW and OW planes can be calculated using,

$$l = r_c + \frac{\frac{\mu_0}{2}\int\int x{\cdot}H_r^2(x,y)\,dx\,dy}{\frac{\mu_0}{2}\int\int H_r^2(x,y)\,dx\,dy} \tag{7}$$

Then the leakage angles across the IW, OW, and transition (TR) regions can be calculated using,

$$\theta_{(\mathrm{IW})} = 2\arcsin\left(\frac{r_c}{w+r_c}\right) \tag{8}$$

$$\theta_{(\mathrm{TR})} = \arcsin\left(\frac{2r_c}{l_{(\mathrm{IW})}+l_{(\mathrm{OW})}}\right) - \frac{\theta_{(\mathrm{IW})}}{2} \tag{9}$$

$$\theta_{(\mathrm{OW})} = \frac{2\pi - s_c\left(\theta_{(\mathrm{IW})}+2\theta_{(\mathrm{TR})}\right)}{s_c} \tag{10}$$

Finally, the partial leakage lengths can be calculated using,

$$d_{(\mathrm{IW})} = l_{(\mathrm{IW})}\left(\theta_{(\mathrm{IW})}+\theta_{(\mathrm{TR})}\right) \tag{11}$$

$$d_{(\mathrm{OW})} = l_{(\mathrm{OW})}\left(\theta_{(\mathrm{OW})}+\theta_{(\mathrm{TR})}\right) \tag{12}$$

Appendix B. Derivation of Dowell's 1-D model Ouyang et al. (2015); Villar (2010)

Maxwell's equations for a divergence-free linear isotropic homogeneous medium with zero displacement current are,

$$\nabla \times E = -\mu_0{\cdot}\frac{\partial H}{\partial t} \tag{13}$$

$$\nabla \times H = \sigma{\cdot}E. \tag{14}$$

For the rectangular foil in Fig. 4, assuming that the electric field intensity E has only $z-$ component and the magnetic field intensity H has only y-component, E and H become functions of x only. Then, the Maxwell's equations in phasor form can be expressed as,

$$\frac{dE_z}{dx} = j\omega\mu_0 H_y \tag{15}$$

$$\frac{dH_y}{dx} = \sigma E_z. \tag{16}$$

Using the above two equations, the Helmholtz second-order differential equation is reached below,

$$\frac{d^2H_y}{dx^2} = j\omega\mu_0\sigma H_y. \tag{17}$$

The general solution of the Helmholtz equation is given by,

$$H_y(x) = H_1 e^{\gamma x} + H_2 e^{-\gamma x} \tag{18}$$

where γ is the propagation constant expressed as,

$$\gamma = \frac{1+j}{\delta} \tag{19}$$

and H_1 and H_2 are constants that can be obtained from the boundary conditions of the foil as,

$$H_1 = \frac{H_y^{ext} e^{-\gamma x_{int}} - H_y^{int} e^{-\gamma x_{ext}}}{2\sinh(\gamma t_w)} \tag{20}$$

$$H_2 = \frac{H_y^{int} e^{\gamma x_{ext}} - H_y^{ext} e^{\gamma x_{int}}}{2\sinh(\gamma t_w)}. \tag{21}$$

By substituting H_1 and H_2 in the general solution above, a frequency-dependent expression is reached that considers only the axial component of magnetic field intensity across the foil,

$$H_y(x) = H_y^{ext}\frac{\sinh(\gamma x)}{\sinh(\gamma t_w)} - H_y^{int}\frac{\sinh(\gamma(x-t_w))}{\sinh(\gamma t_w)}. \tag{22}$$

Finally, the frequency-dependent magnetic energy across the foil shown in Fig. 4 can be calculated using,

$$E_{\text{foil}} = \frac{\mu_0 h_w d_w}{2}\int_0^{t_w} H_y^2(x)\,dx \tag{23}$$

After some mathematical manipulations, (4) can be reached.

Appendix C. Modeling of rectangular foils Sharma and Kimball (2021a)

With reference to Fig. 20, the magnetic field intensity at any point N(x,y) inside or outside the cross-sectional area of the foil of height $2a$ and thickness $2b$, whose center is located at (p,q) is given by,

$$H_N^x = \frac{I}{8\pi ab}\Big((y-q+b)(\beta_1-\beta_2) - (y-q-b)(\alpha_1-\alpha_2). \\ .+ (x-p+a)\ln\frac{s_2}{r_2} - (x-p-a)\ln\frac{s_1}{r_1}\Big) \tag{24}$$

$$H_N^y = \frac{-I}{8\pi ab}\Big((x-p+a)(\beta_2-\alpha_2) - (x-p-a)(\beta_1-\alpha_1). \\ .+ (y-q+b)\ln\frac{s_2}{s_1} - (y-q-b)\ln\frac{r_2}{r_1}\Big) \tag{25}$$

where I is the current through the foil. $\alpha_1,\alpha_2,\beta_1,\beta_2$ must be strictly maintained within $(-\pi,\pi)$ range.

References

Bahmani, M. A., & Thiringer, T. (2015). Accurate evaluation of leakage inductance in high-frequency transformers using an improved frequency-dependent expression. *IEEE Transactions on Power Electronics, 30*(10), 5738–5745. https://doi.org/10.1109/TPEL.2014.2371057

Dang, Y., Zhu, L., Liu, J., Zhan, C., Long, L., & Ji, S. (2022). Module integral method for the calculation of frequency-dependent leakage inductance of high-frequency transformers. *IEEE Transactions on Power Electronics, 37*(6), 7028–7038. https://doi.org/10.1109/TPEL.2022.3141242

Dowell, P. L. (1966). Effects of eddy currents in transformer windings. *Proceedings of the Institution of Electrical Engineers, 113*(8), 1387-1394. https://doi.org/10.1049/piee.1966.0236

Duppalli, V. S., & Sudhoff, S. (2017). Computationally efficient leakage inductance calculation for a high-frequency core-type transformer. *2017 IEEE electric ship technologies symposium (ESTS)* (pp. 635–642). https://doi.org/10.1109/ESTS.2017.8069348

Eslamian, M., & Vahidi, B. (2012). New methods for computation of the inductance matrix of transformer windings for very fast transients studies. *IEEE Transactions on Power Delivery, 27*(4), 2326–2333. https://doi.org/10.1109/TPWRD.2012.2204905

Fouineau, A., Raulet, M.-A., Lefebvre, B., Burais, N., & Sixdenier, F. (2018). Semi-analytical methods for calculation of leakage inductance and frequency-dependent resistance of windings in transformers. *IEEE Transactions on Magnetics, 54*(10), 1–10. https://doi.org/10.1109/TMAG.2018.2858743

Garcia-Bediaga, A., Villar, I., Rujas, A., Mir, L., & Rufer, A. (2017). Multiobjective optimization of medium-frequency transformers for isolated soft-switching converters using a genetic algorithm. *IEEE Transactions on Power Electronics, 32*(4), 2995–3006. https://doi.org/10.1109/TPEL.2016.2574499

Gerling, D. (2009). Approximate analytical calculation of the skin effect in rectangular wires. *2009 international conference on electrical machines and systems* (pp. 1–6). https://doi.org/10.1109/ICEMS.2009.5382786

Gomez, P., & de Leén, F. (2011). Accurate and efficient computation of the inductance matrix of transformer windings for the simulation of very fast transients. *IEEE Transactions on Power Delivery, 26*(3), 1423–1431. https://doi.org/10.1109/TPWRD.2011.2104370

Gu, L., Fan, H., Jin, Z., & Xu, D. (2022). Multi-objective-optimized parameter design method for high-frequency resonant converters. *2022 IEEE energy conversion congress and exposition (ECCE)*.

Guo, X., Li, C., Zheng, Z., & Li, Y. (2022). General analytical model and optimization for leakage inductances of medium-frequency transformers. *IEEE Journal of Emerging and Selected Topics in Power Electronics, 10*(4), 3511–3524. https://doi.org/10.1109/JESTPE.2021.3062019

Hurley, W. G., & Wilcox, D. J. (1994). Calculation of leakage inductance in transformer windings. *IEEE Transactions on Power Electronics, 9*(1), 121–126. https://doi.org/10.1109/63.285502

Kaijia, T., Zhijun, Y., Xiaoming, L., & Liangliang, H. (2019). Analytical calculation of leakage reactance in high-frequency transformers considering frequency-dependent and winding-structure characteristics. *2019 IEEE 3rd international electrical and energy conference (CIEEC)* (pp. 126–130). https://doi.org/10.1109/CIEEC47146.2019.CIEEC-201983

Lambert, M., Sirois, F., Martinez-Duro, M., & Mahseredjian, J. (2013). Analytical calculation of leakage inductance for low-frequency transformer modeling. *IEEE Transactions on Power Delivery, 28*(1), 507–515. https://doi.org/10.1109/TPWRD.2012.2225451

Magot, D., Margueron, X., & Keradec, J. P. (2004). Peec-like analytical calculation of static leakage inductances of h.f. transformers, *vol. 1. Conference record of the 2004 IEEE industry applications conference, 2004. 39th IAS annual meeting.* (p. 545). https://doi.org/10.1109/IAS.2004.1348457

Margueron, X., Keradec, J.-P., & Besri, A. (2007a). Complete analytical calculation of static leakage parameters. Application to HF Transformer Optimization. *2007 IEEE industry applications annual meeting* (pp. 1794–1801). https://doi.org/10.1109/07IAS.2007.274

Margueron, X., Keradec, J.-P., & Magot, D. (2007b). Analytical calculation of static leakage inductances of HF transformers using PEEC formulas. *IEEE Transactions on Industry Applications, 43*(4), 884–892. https://doi.org/10.1109/TIA.2007.900449

McLyman, C. W. T. (2004). *Transformer and inductor design handbook*. CRC Press.

Mogorovic, M., & Dujic, D. (2017). Medium frequency transformer leakage inductance modeling and experimental verification. *2017 IEEE energy conversion congress and exposition (ECCE)* (pp. 419–424). https://doi.org/10.1109/ECCE.2017.8095813

Mogorovic, M., & Dujic, D. (2019). 100 kW, 10 kHz medium-frequency transformer design optimization and experimental verification. *IEEE Transactions on Power Electronics, 34*(2), 1696–1708. https://doi.org/10.1109/TPEL.2018.2835564

Niemela, V. A., Skutt, G. R., Urling, A. M., Chang, Y.-N., Wilson, T. G., Owen, H. A., & Wong, R. C. (1989). Calculating the short-circuit impedances of a multiwinding transformer from its geometry, *vol.2. 20th annual IEEE power electronics specialists conference* (pp. 607–617). https://doi.org/10.1109/PESC.1989.48541

Ouyang, Z., Hurley, W. G., & Andersen, M. A. E. (2019). Improved analysis and modeling of leakage inductance for planar transformers. *IEEE Journal of Emerging and Selected Topics in Power Electronics, 7*(4), 2225–2231. https://doi.org/10.1109/JESTPE.2018.2871968

Ouyang, Z., Zhang, J., & Hurley, W. G. (2015). Calculation of leakage inductance for high-frequency transformers. *IEEE Transactions on Power Electronics, 30*(10), 5769–5775. https://doi.org/10.1109/TPEL.2014.2382175

Prieto, R., Cobos, J. A., Garcia, O., Alou, P., & Uceda, J. (2003). Study of 3-D magnetic components by means of "double 2-D" methodology. *IEEE Transactions on Industrial Electronics, 50*(1), 183–192. https://doi.org/10.1109/TIE.2002.807663

Schlesinger, R., & Biela, J. (2020). Leakage inductance modelling of transformers: Accurate and fast models to scale the leakage inductance per unit length. *2020 22nd european conference on power electronics and applications (EPE'20 ECCE Europe)* (pp. P.1–P.11). https://doi.org/10.23919/EPE20ECCEEurope43536.2020.9215756

Schlesinger, R., & Biela, J. (2021). Comparison of analytical models of transformer leakage inductance: Accuracy versus computational effort. *IEEE Transactions on Power Electronics, 36*(1), 146–156. https://doi.org/10.1109/TPEL.2020.3001056

Sharma, A., & Kimball, J. W. (2021a). Evaluation of transformer leakage inductance using magnetic image method. *IEEE Transactions on Magnetics, 57*(11), 1–12. https://doi.org/10.1109/TMAG.2021.3111479

Sharma, A., & Kimball, J. W. (2021b). Novel transformer with variable leakage and magnetizing inductances. *2021 IEEE energy conversion congress and exposition (ECCE)* (pp. 2155–2161). https://doi.org/10.1109/ECCE47101.2021.9595797

Sharma, A., & Kimball, J. W. (2022). New hybrid model for evaluating the frequency-dependent leakage inductance of a variable inductance transformer (VIT). *2022 IEEE energy conversion congress and exposition (ECCE)*.

Sullivan, C. R. (1999). Optimal choice for number of strands in a Litz-wire transformer winding. *IEEE Transactions on Power Electronics, 14*(2), 283–291. https://doi.org/10.1109/63.750181

Tan, W., Margueron, X., Taylor, L., & Idir, N. (2016). Leakage inductance analytical calculation for planar components with leakage layers. *IEEE Transactions on Power Electronics, 31*(6), 4462–4473. https://doi.org/10.1109/TPEL.2015.2471090

Villar, I. (2010). *Multiphysical characterization of medium-frequency power electronic transformers*. EPFL Lausanne, Switzerland. Ph.D. thesis.

Wilcox, D. J., Conlon, M., & Hurley, W. G. (1988). Calculation of self and mutual impedances for coils on ferromagnetic cores. *IEE Proceedings A-Physical Science, Measurement and Instrumentation, Management and Education-Reviews, 135*(7), 470–476.

Zhang, K., Chen, W., Cao, X., Pan, P., Azeem, S. W., Qiao, G., & Deng, F. (2020). Accurate calculation and sensitivity analysis of leakage inductance of high-frequency transformer with Litz wire winding. *IEEE Transactions on Power Electronics, 35*(4), 3951–3962. https://doi.org/10.1109/TPEL.2019.2936523